Mech. Adv. Technol. Vol. 6, No. 1, 2022, pp. 85–95

DOI: 10.20535/2521-1943.2022.6.1.252889

UDC 532.528

Dynamics of supercavitating vehicles with cone cavitators

V. Semenenko[1] • V. Moroz[1] • V. Kochin[1] • O. Naumova[1]

Received: 15 February 2022 / Accepted: 30 May 2022

Abstract. *The work is devoted to theoretical and experimental investigations of dynamics of high-speed underwater supercavitating vehicles with cone cavitators. The cone cavitators are considered as operating controls of the supercavitating vehicle motion. The mathematical model of a "slender" unsteady cavity based on the G.V. Logvinovich principle of independence of the cavity section expansion is used. Experimental studies of the rotary cone cavitators were carried out at the high-speed experimental tank of the Institute of Hydromechanics of the NAS of Ukraine. Based on test results, the approximate dependences of both the drag coefficient and the lift coefficient of an inclined cone cavitator on the rotary angle in a wide range of cone angles are proposed. The range of cone angles is determined when the cone cavitators are the more effective operating controls in comparison with equivalent disk cavitator. With the help of computer simulation, a number of problems of dynamics of the supercavitating vehicle with cone cavitators were investigated: balancing the vehicle, the motion stabilization, maneuvering the vehicle, the cavity control. For the first time, experimental verification of the mathematical model of the supercavitating vehicle dynamics "as a whole" was performed by testing the model with cone cavitators and cavity-piercing fins with a degree of freedom in pitch.*

Keywords: *supercavitating vehicle, cone cavitator, mathematical model, computer simulation, experimental studies.*

1. Introduction

When motion of high-speed underwater supercavitating vehicles (SC-vehicles), a cavity filled with the water vapor or gas is formed around the vehicle body with the help of a nose cavitator. The disk cavitator is the most studied (see [1]). Recently, an interest in the using the cavitators with other shapes has increased, in particular the cone cavitators. In this case, the cavitator is considered not only as a device for creating a cavity, but also as an operating control of the SC-vehicle motion.

To calculate the parameters of the unsteady flow over SC-vehicles, the mathematical model of the "slender" unsteady cavity was developed. It is based on the *G.V. Logvinovich* principle of independence of the cavity section expansion (see [2−5]). In this mathematical model, to determine the unsteady ventilated cavity pressure and the hydrodynamic forces acting on the SC-vehicle elements, various approximation dependences are used obtained on the basis of theoretical studies and/or experimental data (see [6−9]).

Based on this mathematical model, we developed rapid computational algorithms allowing to observe the SC-model dynamic behavior on the computer screen directly during the calculation, *i.e.* to perform a computer simulation. With the help of computer simulation, the problem of the SC-vehicle speeding-up (see [10, 11]), various methods of control of the SC-vehicle motion (see [4, 12]), as well as peculiarities of the SC-vehicle maneuvering in depth and on course (see [13, 14]) were investigated.

The difficulty in calculating dynamics of SC-vehicles with cone cavitators is caused by absence of a reliable dependence of both the lift coefficient c_y and the drag coefficient c_x of the rotary cavitators on the rotary angle δ. For disk cavitators, such dependences was obtained long ago (see [1, 4]). We are aware of the only work devoted to the experimental study of the flow over supercavitating cones [15]. However, the data given there are not enough

✉ *V. Semenenko*
vnsvns@gmail.com

[1] *Institute of Hydromechanics of the National Academy of Sciences of Ukraine, Kyiv, Ukraine*

to acquisition of the universal dependences $c_y(\delta)$, $c_x(\delta)$ for sufficiently wide range of the cone angles β_n.

To obtain additional experimental data, a test rig based on the high-speed experimental tank of the Institute of Hydromechanics of the National Academy of Sciences of Ukraine was used. Earlier this test rig was used to compare the theoretical and experimental cavity shapes [16] and the transverse force arising when planing the model aft part along the cavity wall [17]. Also for the first time, an experimental verification of the mathematical model of the SC-vehicle dynamics "as a whole" was performed on this test rig by testing models with the disk cavitators and the cone cavitators and the cavity-piercing fins with a degree of freedom in pitch [18].

The purpose of this work is acquisition of the universal dependencies $c_{nx}(\delta)$ and $c_{ny}(\delta)$ for various cone angles β_n, and computer simulation of various aspects of the dynamic behavior of the SC-vehicle with cone cavitators, such as balancing the SC-vehicle, motion stabilization, maneuvering the SC-vehicle, and the cavity control.

2. Experimental study of supercavitating models with cone cavitators

The high-speed experimental tank of the IHM NAS of Ukraine has the length 140 meters, the width 4 meters, and the depth 1.8 meters. Experimental studies were carried out in accordance with the procedure [19] by performing towing tests of cavitator models in the experimental tank in the towing velocity range 7–10 m/s.

Four models of cavitators having a cone shape and a disk shape were tested. All the cavitator models had the same base diameter 50 mm. The cone-shaped cavitators had the cone angle β_n = 40, 60, and 120 degrees. Sketches of the cavitator models are shown in Fig. 1.

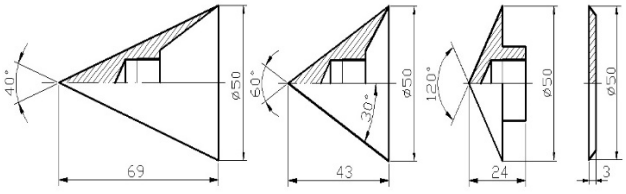

Fig. 1. Sketches of the tested cavitator models

The cavitator models were mounted to a suspension with the help of a threaded adapter. Scheme of the suspension is shown in Fig. 2. The suspension consisted of a hollow pylon, in the upper part of which there were elements for mounting it to the experimental tank towing carriage. The lower end of the pylon was connected to a horizontal pipe with the outer diameter 30 mm.

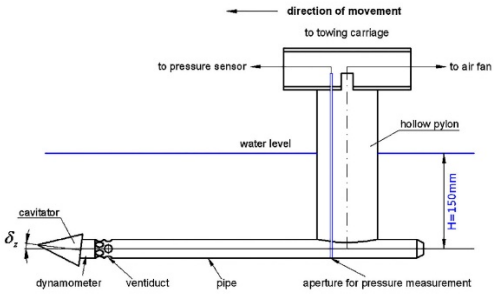

Fig. 2. Scheme of mounting the cavitator model to the suspension

A tensometric dynamometer with a threaded adapter was mounted in the nose part of the pipe. In the experiments, a set of adapters was used ensuring the mounting the cavitator models with the rotary angles $\delta = 0°$; ±7.5° and ±14° relatively to the horizontal pipe axis.

A drainage tube was laid through the internal hollow of the pylon and the pipe. The lower end of the drainage tube was brought inside the cavity, the upper end was connected to a pressure sensor. The cavity pressure was measured using the differential pressure sensor Motorola MPXV5004DP.

The cavitation flow was organized artificially by blowing air into the zone behind the cavitator using a 6-stage axial fan. The air rate was measured using the air flow sensor Honeywell AWM720P1, which was installed at the inlet of the fan.

In these experiments, the air-supply rate was $\dot{Q}_{in} \approx 0.0064 \div 0.0072$ m^3/s. Such air-supply rate made it possible, on the one hand, to achieve the very low cavitation number $\sigma \approx 0.03 \div 0.04$, and on the other hand, to achieve a stable supercavitation flow. In this case, the *Froude* numbers Fr_d calculated with respect to the cavitator diameter were $Fr_d \approx 11.5 \div 14.3$.

The cavitator immersion depth H may by regulated by vertical relocation of the pylon and was set at the level $H = 150$ mm in these experiments.

All the sensors and dynamometer were included in the automated system for collecting and processing information from the experimental tank [20].

To determine the geometric and kinematic parameters of the cavitation flow during experiments, the underwater video recording in the towing carriage coordinates was used. To realize the underwater video recording, an underwater container was moved parallel to the model motion. In this container, a remotely controlled video camera and also illuminators were placed. A SONY DSC-RXO video camera was used, which shot 50 frames per second with resolution 1920×1080 pixels. Fig. 3 shows characteristic views of the cavitation flow past the cone cavitator for various rotary angles. Here δ_z is the cavitator rotary angle in the vertical plane considered positive when the cavitator is turned clockwise.

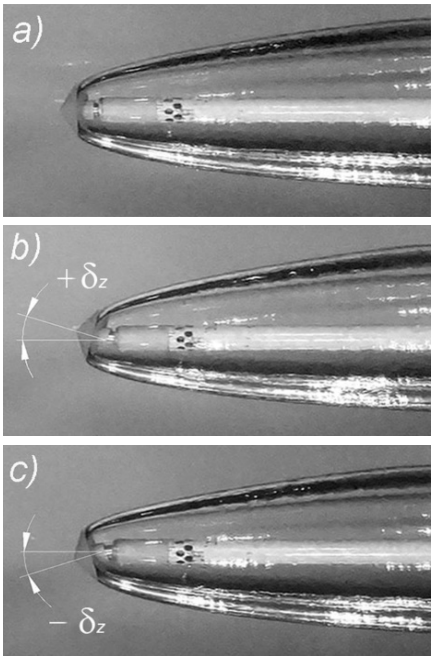

Fig. 3. View of the flow behind the cone cavitator with $\beta_n = 120°$: (*a*) – $\delta_z = 0°$; (*b*) – $\delta_z > 0°$; (*c*) – $\delta_z < 0°$

Fig. 4 shows examples of experimental dependences of both the lift coefficient c_y and the drag coefficient c_x of the cone cavitator (*a*) and the disk cavitator (*b*) on the rotary angle δ_z obtained when $\sigma = 0.05$.

In [21], basing on the analysis of results of the experimental work [15], it was concluded that the lift coefficient of a cone cavitator may be presented in the form:

$$c_y = c_{y0}^{\delta}(1+\sigma)\delta_z, \quad -20° < \delta_z < 20°, \tag{1}$$

where c_{y0}^{δ} is the derivative of the lift coefficient of the cone cavitator with respect to the rotary angle δ_z when $\sigma = 0$.

Fig. 5 shows the universal dependence of the lift coefficient derivative on the cone angle $c_{y0}^{\delta} = f(\beta_n)$ that we obtained. When plotting this curve, we used our experimental results as well as experimental data from [15]. It was also taken into account that the cone degenerates into a cylinder with $c_{y0}^{\delta} = 2$ when $\beta_n \to 0°$, and the cone degenerates into a disk with $c_{y0}^{\delta} = 0.783$ when $\beta_n \to 180°$, if the rotary angle is set in radians (see [1]).

For the convenience of practical using, we approximated dependence Fig. 5 by a polynomial of the third degree:

$$c_{y0}^{\delta} = 2.05\cdot10^{-7}\beta_n^3 + 1.355\cdot10^{-4}\beta_n^2 - \\ -3.325\cdot10^{-2}\beta_n + 2.0. \tag{2}$$

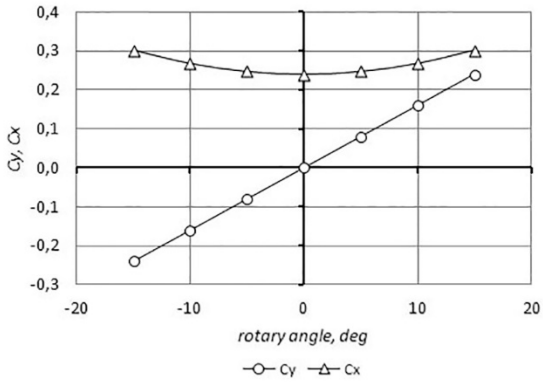

a

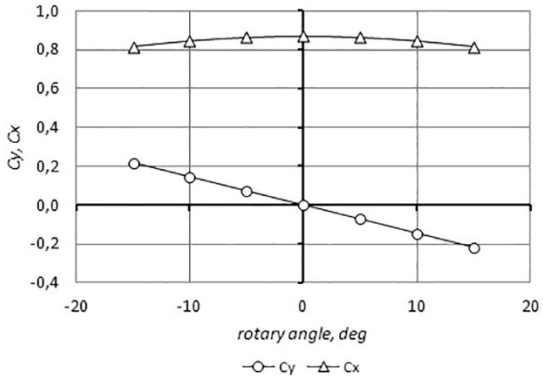

b

Fig. 4. Experimental dependences c_y and c_x on δ_z: (*a*) – $\beta_n = 40°$; (*b*) – $\beta_n = 180°$ (disk)

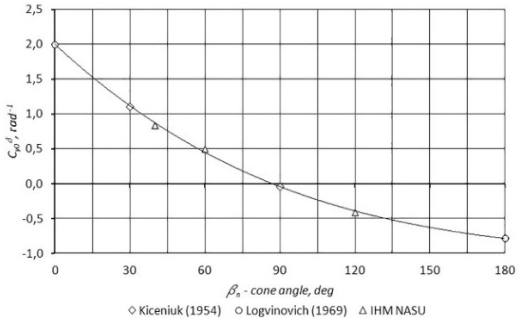

Fig. 5. Dependence $c_{y0}^{\delta} = f(\beta_n)$

For the drag coefficient of an inclined cone cavitator, we proposed the semi-empirical formula:

$$c_x(\delta_z) = c_{x1} + c_y \sin\delta_z \tag{3}$$

where c_{x1} is the drag coefficient of the cone cavitator when $\delta_z = 0$ (see below formulae (12), (13)). Formula (3) is agreed with our experimental data in the range $-15° < \delta_z < 15°$, and with the experimental data from [15] as well.

3. Mathematical model

Computer simulation of the SC-vehicle motion is performed by numerical integration of the set of equations including:

1) the differential equations of an axisymmetric rigid body 6-DOF dynamics (see [4]);

2) the equations to calculate an unsteady cavity shape and position based on the *G.V. Logvinovich* principle of independence of the cavity section expansion (see [2–4]);

3) the equation of the mass of gas in the cavity balance for the ventilated cavity (see [6, 11]);

4) the relations for hydrodynamic forces acting on the inclined cavitator (see [4]);

5) the relations for hydrodynamic forces acting when the vehicle body interacts with

the cavity walls (planing or ricochet, see [9, 14]);

6) the relations for hydrodynamic forces acting on the cavity-piercing fns (see [5, 12]).

To calculate the shape of the cavity behind the cone cavitator, the equivalent disk cavitator method is used [22]. Cavitators with various shapes are called equivalent ones, if $D_n\sqrt{c_{x0}} = const$. The cavities formed behind the equivalent cavitators will have the same main dimensions for the same cavitation number σ [22]:

$$D_c = D_n\sqrt{\frac{c_{x0}(1+\sigma)}{\kappa\sigma}}, \quad L_c = D_n\frac{A\sqrt{c_{x0}}}{\sigma}, \tag{4}$$

where D_c and L_c are the cavity maximal diameter and the cavity length, respectively; $\kappa = 0.96$, $A = 2.0$ are the empirical constants. The diameter of the equivalent disk cavitator is equal to:

$$D_n^{(e)} = \frac{D_n}{\gamma}, \quad \gamma = \sqrt{\frac{0.8275}{c_{x0}}}, \tag{5}$$

where D_n is the cone base diameter; $c_{x0}(\beta_n)$ is the cavitation drag coefficient of the cone when $\sigma = 0$.

Thus, to calculate the shape of the steady axisymmetric cavity behind the cone cavitator, one can use the composite cavity formulae obtained for the disk cavitator [1, 3]:

$$S(x) = S_n\left(1+\frac{3x}{R_n}\right)^{\frac{2}{3}}, \qquad x \le x_1, \tag{6}$$

$$S(x) = S_1 + k_1\frac{x-x_1}{2}\left(R_n A\sqrt{c_{x0}} - \sigma_0\frac{x-x_1}{2}\right), x_1 < x \le L_c \tag{7}$$

Where S is the cavity cross-section area; $x_1 = D_n$ is the length of the frontal cavity part; $R_n = D_n/2$ is the cavitator base radius; $S_n = \pi R_n^2$ is the cavitator base area; $S_1 = S(x_1)$ is the area of the "agreement section" of the frontal cavity part and the main cavity part; $k_1 = 4\pi/A^2$.

Calculations have shown that formula (6) can be used when $90° \le \beta_n \le 180°$. In the case of the "sharper" cone cavitators $30° \le \beta_n \le 90°$ we proposed the empirical formula instead of (6):

$$S(x) = S_n\left(1+\tan\frac{\beta_n}{2}\frac{3x}{R_n}\right)^{\frac{2}{3}}, \qquad x \le x_1. \tag{8}$$

The deformation of the cavity axis under the action of the lift on the cone cavitator $h_f(x)$ and under the action of buoyancy $h_g(x)$ is calculated by generalizing the approximation formulae obtained for the disk cavitator [7]:

$$h_f(x) = -\gamma c_y R_n\left(0.46-\sigma+2\bar{x}\right), \; c_y = \frac{8F_{ny}}{\rho V^2\pi D_n^2}, \tag{9}$$

$$\bar{h}_g(x) = L_c\frac{(1+\sigma)\bar{x}^2}{3Fr_l^2}, \quad Fr_l = \frac{V_\infty}{\sqrt{gL_c}}, \tag{10}$$

where $\bar{x} = x/L_c$; Fr_l is the *Froude* number with respect to the cavity length.

Formulae (6)–(10) are generalized to the case of unsteady cavities using the *G.V. Logvinovich* principle of independence of the cavity section expansion (see [2, 3]).

The cone cavitator drag F_{nx} when $\delta_z = 0$ consists of two parts: the pressure (cavitation) drag F_{nx1} and the skin friction drag F_{nx2} [23]:

$$F_{nx} = F_{nx1} + F_{nx2} = \frac{\rho V^2}{2}\frac{\pi D_n^2}{4}\left(c_{x1} + \frac{c_f}{\sin\frac{\beta_n}{2}}\right), \tag{11}$$

where $c_f(\mathrm{Re})$ is the viscous drag coefficient; Re is the *Reynolds* number with respect to the cone generatrix length. For the cavitation drag coefficient, the *Reichardt* formula is valid when the cone angle β_n is not too small [22]:

$$c_{x1}(\beta_n, \sigma) = c_{x0}(\beta_n)(1+\sigma), \tag{12}$$

where c_{x0} is the cone cavitation drag coefficient when $\sigma = 0$. The coefficient c_{x0} in dependence on the cone angle β_n is calculated by approximating the numerical calculation [8]:

$$c_{x0} = 0.5 + 1.81(\beta_n/360 - 0.25) - 2(\beta_n/360 - 0.25)^2, \quad 30° \le \beta_n \le 180° \tag{13}$$

The viscous drag coefficient c_f is calculated using known formulae for the boundary layer [24]. The skin friction drag proportion is the more the less is β_n.

The drag coefficient of the inclined cone cavitator c_x is calculated by formula (3).

The lift coefficient of the inclined cone cavitator c_y is calculated by formulae (1), (2) in the range $-20° \le \delta_z \le 20°$. Note that it follows from (2) that $c_{y0}^{\delta} = 0$ when $\beta_n = 86.85°$. This value of the cone angle may be called as critical one $\beta_n^{(cr)}$. It is obvious that cone cavitators with the cone angles close to the critical value $\beta_n^{(cr)}$ cannot be used for the SC-vehicle motion control.

Note also that there is a theoretical solution to the plane nonlinear problem of cavitation flow around a wedge, which gives a qualitatively similar dependence $c_{y0}^{\delta}(\beta_n)$ [25]. In this case the critical value is $\beta_n^{(cr)} = 101.17°$.

Table 1 gives values of the dimensionless parameters γ, c_{x0} and c_{y0}^{δ} calculated by formulae (5), (13), (2), respectively, for a number of the cone angles β_n.

4. Efficiency of cone cavitators as operating controls

Let us consider a problem of efficiency of using the cone cavitators to control of the SC-vehicle motion. We consider a series of the cone cavitators with various cone angles β_n, corresponding to the equivalent disk cavitator with the same diameter $D_n^{(e)}$. Base diameters of the equivalent cone cavitators D_n in dependence on β_n are determined by formula (4). Each of the cone cavitators generates the lift:

$$F_{ny} = \frac{\rho V^2}{2}\frac{\pi D_n^2}{4} c_{y0}^{\alpha}(1+\sigma)\delta_z =$$

$$= \frac{\rho V^2}{2}\frac{\pi D_n^{(ef)2}}{4}\frac{0.8275}{c_{x0}(\beta_n)} c_{y0}^{\alpha}(\beta_n)(1+\sigma)\delta_z . \qquad (14)$$

As can be seen, this force *i.e.* efficiency of the cone cavitator as an operating control for fixed values of V, σ, $D_n^{(e)}$, δ_z and various β_n differs only by the dimensionless factor:

$$\mu(\beta_n) = \frac{c_{y0}^{\delta}}{c_{x0}} . \qquad (15)$$

Fig. 6 gives graphs of dependence of the coefficients c_{x0}, c_{y0}^{δ}, and μ on β_n. For the disk cavitator one has $|\mu| = 0.946$. For the cone cavitator one has $\mu > 0.946$ when $\beta_n < 65.4°$. Thus, one can say that when $\beta_n < 65.4°$, the cone cavitators are the more efficient operating controls than the equivalent disk cavitator. Their advantage increases rapidly with decreasing the cone angle. For example when $\beta_n = 60°$, the cone cavitator efficiency is higher on 41.5 %, and when $\beta_n = 40°$, its efficiency is higher in 4.4 times.

In practice, as experiments [15] show, the dependence $c_{ny}(\delta)$ becomes non-monotonic when $\beta_n < 40°$. This is explained by the displacement of the cavity detachment line from the cone base to the cone leeward side, similarly to as it occurs during the cavitation flow around a flat wedge [25]. In these cases, formulae (1), (2) may not be applied.

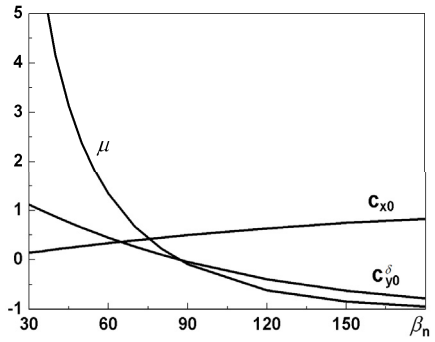

Fig. 6. Dependence of the coefficients c_{x0}, c_{y0}^{δ}, μ on β_n

5. Calculation model and calculation parameters

Below are examples of calculating the steady and unsteady regimes of motion of the SC-model with cone cavitators. All calculations were performed for the SC-vehicle model showed in Fig. 7. Its main parameters are: the

Table 1. Coefficients γ, c_{x0}, c_{y0}^{δ} in dependence on β_n

β_n°	30.0	40.0	60.0	80.0	90.0	120.0	150.0	180.0
γ	2.4072	1.9851	1.5710	1.3588	1.2865	1.1399	1.0531	1.0000
c_{x0}	0.1428	0.2100	0.3353	0.4482	0.5000	0.6369	0.7461	0.8275
c_{y0}^{δ}	1.119	0.874	0.449	0.102	-0.044	-0.393	-0.631	-0.783

length L = 5.0 m, the cylindrical part diameter D_b = 340 mm, the mass m = 600 kg, the mass center position x_c = 3.0 m, moments of inertia about the vehicle axes I_x = 8.0 kg m^2, $I_y = I_z$ = 900.0 kg m^2.

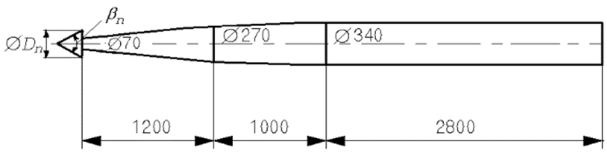

Fig. 7. Design scheme of the SC-vehicle model

The starting parameters of the model motion (unless otherwise specified) are: the velocity V = 120 m/s, the immersion depth H = 10 m. In this case, the cavitation number is σ = 0.02, the cavity length is L_c = 6.565 m, the volumetric gas-supply rate into the cavity is $\dot{Q}_{in}$ = 72.125 l/s.

The calculations were performed for a number of cone cavitators equivalent to the disk cavitator with diameter $D_n^{(e)}$ = 70 mm. The cavitator cone angle β_n may be varied from 30° to 180° (disk). Table 2 shows values of the diameters D_n (4) and the total drag F_{nx} (11) of the cone cavitators for a number of the cone angles β_n.

6. Balancing the SC-vehicles with cone cavitators

The steady longitudinal motion of the SC-vehicle is called the balanced one, if sums of all the forces acting and their moments relative to the vehicle mass center are equal to zero. To determine the balanced values of parameters, one applies an iterative numerical algorithm developed in our work [11].

Table 3 shows the balanced values of the cavitator rotary angle δ_z and the model pitch angle ψ (in degrees) for this calculation model with a number of the cone cavitators equivalent to the disk cavitator with $D_n^{(e)}$ = 70 mm.

As can be seen from the Table 3, the function $\delta_z^*(\beta_n)$ has a discontinuity when transiting through the critical value $\beta_n = \beta_n^{(cr)} = 86.85°$. For the cone angles close to the critical one balancing the SC-model is impossible.

Fig. 8, *a, b* shows graphs of dependence of the balanced parameters δ_z^*, ψ^* (in degrees) on the model mass center position $\bar{x}_c = x_c / L$ for the disk cavitator $\beta_n = 180°$ and for a number of equivalent cone cavitators. As can be seen, these dependencies are linear for any cone angle.

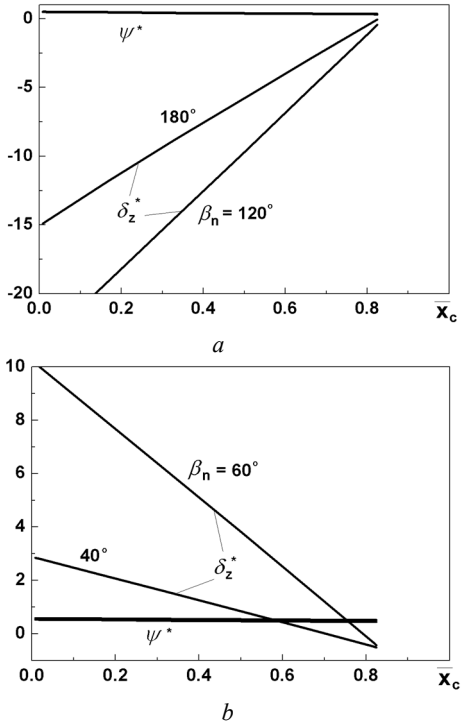

Fig. 8. Balanced values of angles δ_z^*, ψ^* depending on x_c : *a* – $\beta_n > \beta_n^{(cr)}$; *b* – $\beta_n < \beta_n^{(cr)}$

Table 2. Values D_n and F_{nx} of the cone cavitators in dependence on β_n

β_n°	30.0	40.0	60.0	80.0	90.0	120.0	150.0	180.0
D_n, mm	168.52	138.95	109.97	95.12	90.05	79.79	73.72	70.00
F_{nx}, KN	25.113	24.346	23.840	23.672	23.622	23.550	23.515	23.165

Table 3. Balanced values of angles δ_z^*, ψ^* depending on β_n

β_n°	30.0	40.0	60.0	80.0	90.0	120.0	150.0	180.0
δ_z^*	0.1008	0.8356	3.8168	24.6956	-65.1021	-9.7079	-7.1789	-5.7742
ψ^*	0.6282	0.5377	0.4734	0.4601	0.4621	0.4083	0.3891	0.3725

7. Stabilization of motion of SC-vehicles with cone cavitators

As is known, the longitudinal motion of a balanced SC-vehicle with a disk cavitator in the planing in a cavity regime is unstable in depth (see [4]). In [26] one proposed an algorithm for active stabilization of the SC-vehicle motion by regulating the disk cavitator rotary angle δ_z, which operates on the feedback principle:

$$\delta_z(t) = \delta_z^* + k_1 y(t) + k_2\left[\psi(t) - \psi^*\right] - k_3\omega_z(t), \quad (16)$$

where y is displacement of the model mass center in depth; ω_z is the angular velocity of the model; $k_1 \geq 0$, $k_2 \geq 0$, and $k_3 \geq 0$ are the feedback coefficients.

The calculations showed that the motion of the balanced SC-vehicle with the cone cavitators in the planing in the cavity regime is also unstable for any β_n (see Fig. 9, *a*). In this case, the stabilization algorithm (16) is applicable for the cone cavitators when $\beta_n^{(cr)} < \beta_n < 180°$. When rotating the cone cavitator with the cone angle $\beta_n < \beta_n^{(cr)}$, the arising lift reverses the sign (see formula (2)). Therefore, in this case, the feedback law for regulating the cone cavitator rotary angle should be given in the form:

$$\delta_z(t) = \delta_z^* - k_1 y(t) - k_2\left[\psi(t) - \psi^*\right] + k_3\omega_z(t), \quad \beta < 86.85°. \quad (17)$$

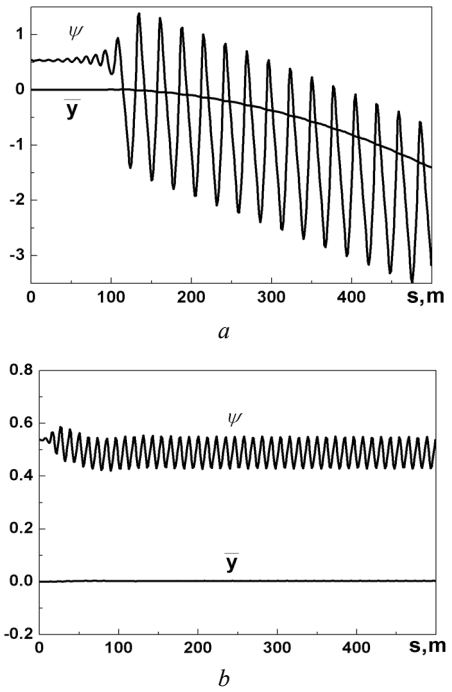

Fig. 9. Varying the pitch angle ψ and deflection of the model mass center y: (*a*) – without stabilization; (*b*) – with stabilization (17)

Obviously, for the cone angles close to the critical value $\beta_n = \beta_n^{(cr)} = 86.85°$ this motion stabilization system will not work.

Fig. 9, *a, b* shows the graphs of varying the model pitch angle ψ (in degrees) and the dimensionless deflection of the model mass center from the horizontal path on the distance $s = 500$ m.

The calculation was performed for the model with the cone cavitator $\beta_n = 40°$ at the balanced starting values of the angles δ_z, ψ from Table 3. When calculating the variant (*b*), the automatic system for the motion depth-stabilization (17) with the parameters $k_1 = 2.0$, $k_2 = 5.0$, $k_3 = 10.0$ was turned on. As one can see, the automatic motion stabilization system operates effectively for the SC-model with the cone cavitator.

8. Maneuvering the SC-vehicles with cone cavitators

Fig. 10, *a*, *b* shows the calculated paths of the model mass center in the vertical plane for a number of the cone cavitator rotary angles δ_z (the so-called δ-control) on the distance $s = 500$ m. The calculations were performed for two cone angles $\beta_n = 40°$ and $\beta_n = 60°$. The starting values of the parameters δ_z, ψ were equal to their balanced values from Table 3. In the case $\beta_n = 40°$, $\delta_z = 1.2°$, the model reached the water surface after flying the distance 416 m. In the case $\beta_n = 60°$, $\delta_z = 4.3°$, the model reached the water surface after flying the distance 474 m.

Fig. 11, *a*, *b* shows the projections of the path of the model mass center onto the horizontal plane for a number of the cone cavitator rotary angles in the horizontal plane δ_y on the distance $s = 500$ m. The starting values of the parameters δ_z, ψ were equal to their balanced values from Table 3. During the calculations, the automatic stabilization system (17) with the parameters $k_1 = 2.0$, $k_2 = 5.0$, $k_3 = 10.0$ was turned on. That ensured the small deflections of the SC-model in depth.

Comparison of graphs in Fig. 10 and Fig. 11 confirms the higher efficiency of the cone cavitator $\beta_n = 40°$ when maneuvering the SC-model both in depth and on course compared to the cone cavitator $\beta_n = 60°$, which is more efficient by-turn than the equivalent disk cavitator with $D_n = 70$ mm.

Note that the approach based on the feedback principle, described in Section 7, makes it possible to develop algorithms for automatic control of the SC-vehicle motion that ensures their motion along assigned (program) paths (see [27]). As the computer simulation has shown, the simultaneous independent regulation of both the cavitator ro-

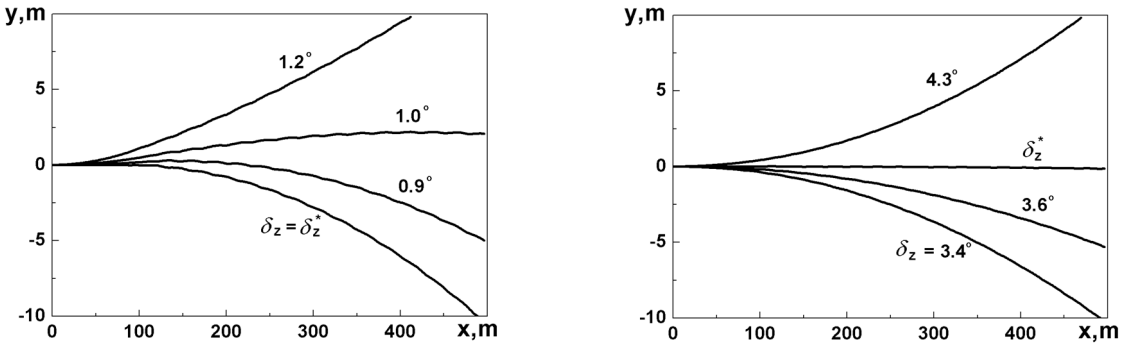

a *b*

Fig. 10. The SC-model paths at the δ-control in depth (*a*) – $\beta_n = 40°$; (*b*) – $\beta_n = 60°$

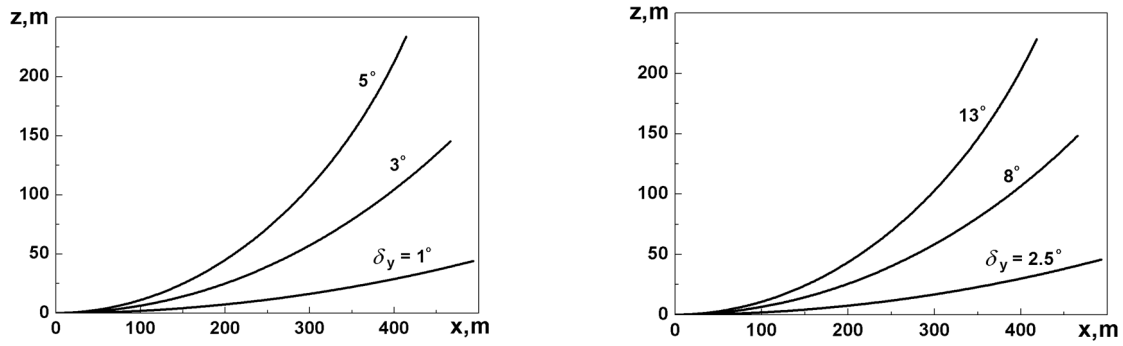

a *b*

Fig. 11. The SC-model paths at the δ-control on course (*a*) – $\beta_n = 40°$; (*b*) – $\beta_n = 60°$

tary angle δ_z proportionally to displacement of the immersion depth $y(t)$ and the path angle $\vartheta(t) = \psi - \alpha$, and the deflection angle of the vertical cavity-piercing fins proportionally to the deflection of the path angle $\chi(t) = \phi - \beta_y$ is quite effective in this case (here ψ, ϕ, α, β_y are the pitch, yaw, attack, sliding angles, respectively).

9. Cavity control by the cavitator cone angle regulation

Theoretically, it is possible to propose a method for active control of the SC-vehicle cavity dimensions by regulating the cavitator cone angle β_n for the fixed cavitator diameter D_n. Note that another type of the variable-drag cavitator was proposed and realized experimentally in [28].

When β_n is varied, the SC-vehicle may be flown around in one of two cavitation regimes. In the partial cavitation regime, the vehicle drag is a sum of the cavitator drag F_{nx} and the skin friction drag of the wetted part of the body F_{bx} (see [10, 11]). In the regime with free closure of a cavity, the SC-vehicle drag is equal to F_{nx}. These force coefficients are defined by formulae:

$$F_{nx} = \frac{\rho V^2}{2}\frac{\pi D_n^2}{4} c_{nx}, \; F_{bx} = \frac{\rho V^2}{2}\frac{\pi D_n^2}{4} c_{bx}. \qquad (18)$$

Fig. 12, *a* shows graphs of varying the dimensionless cavity length $L_c' = L_c / L$ and dimensionless cavity pressure $p_c' = 2p_c / \rho V_0^2$ when stepwise varying the angle β_n. In this case, the cone angle increases from 60° to 90° per 1s. Graphs of β_n variation (in radians) are plotted with dash-dotted lines. Fig. 12, *b* shows graphs of respective varying the coefficients of the model drag components c_{nx}, c_{bx}, and the total drag coefficient c_x.

As can be seen, the cavity reaction onto the β_n variation is of a delayed nature. For periodic β_n variation, this appears in a phase shift of the cavity oscillation. The cavitation drag increases with increasing β_n, and the skin friction drag decreases due to decreasing the wetted surface of the model. In this case, the total drag decreases as well.

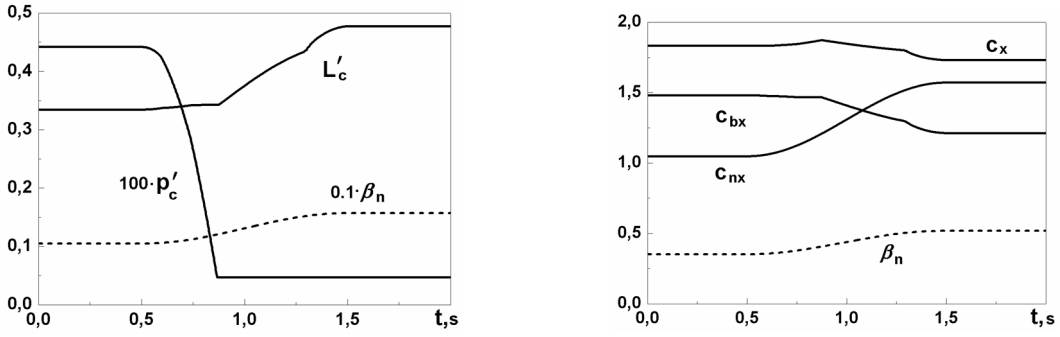

a *b*

Fig. 12. The flow parameters for stepwise variation of β_n : (*a*) – variation of L_c and p_c ; (*b*) – variation of c_{nx} c_{bx} , c_x

By regulating the cavitator cone angle $\beta_n(t)$, it is possible to compensate varying the cavity dimensions caused by varying the velocity $V(t)$ and/or the immersion depth $H(t)$ of the SC-vehicle motion (within certain limits). Fig. 13 shows an example of calculating the compensation of decreasing the ventilated cavity length caused by stepwise increasing the immersion depth $H(t)$ (the dash-dotted line) from 5 m to 10 m per 5 s by stepwise increasing the cone angle $\beta_n(t)$ from 60° to 89° (β_n plotted in radians). During the regulation, the total model drag increased due to the cavitation drag growth.

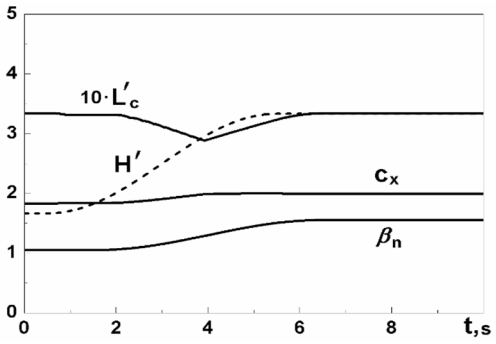

Fig. 13. Compensation of the immersion depth increase by regulating the cavitator cone angle

10. Experimental verification of mathematical model

Since the developed mathematical model of the SC-vehicle dynamics is approximation one, its experimental verification is an urgent problem. As a rule, the model experiments are carried out in hydrodynamic tunnels with fixed models. Such studies are well appropriate for checking the correctness of determining the cavity shape and the hydrodynamic forces acting on the SC-vehicle elements. However, to verify the reliability of the mathematical model of the SC-vehicle dynamics "as a whole", it is necessary to carry out experiments when the model has the ability to move freely under the action of hydrodynamic forces.

On the test rig described above, the mathematical model of the SC-vehicle dynamics "as a whole" was verified by comparing the calculated kinematic parameters obtained in the computer simulation with similar parameters obtained during towing tests (see [18]). In this case, the model with disk and cone cavitators and the cavity-piercing fins with one degree of freedom in pitch were tested (see Fig. 14).

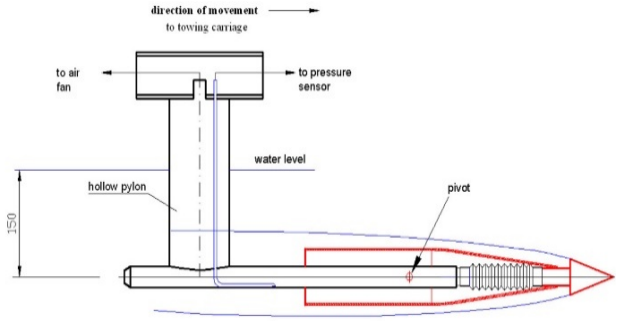

Fig. 14. Scheme of suspension of the model with a degree of freedom in pitch

During the tests, the following three regimes of the SC-vehicle model motion were recorded in dependence on the starting data:

1) the steady planing of the model along the lower cavity wall;

2) the steady planing of the model along the upper cavity wall (see Fig. 15);

3) the unsteady regime, when the model performs angular oscillation ricocheting by turns from the upper and the lower cavity walls with the frequency f = 4.6 Hz.

In all the three cases, satisfactory qualitative and quantitative agreement between the results of physical modelling and computer simulations was obtained. This indicates the adequacy of the relations used to calculate the

forces on the cone cavitators, the forces arising at the interaction of the model body with the cavity walls, and the forces on the cavity-piercing fins.

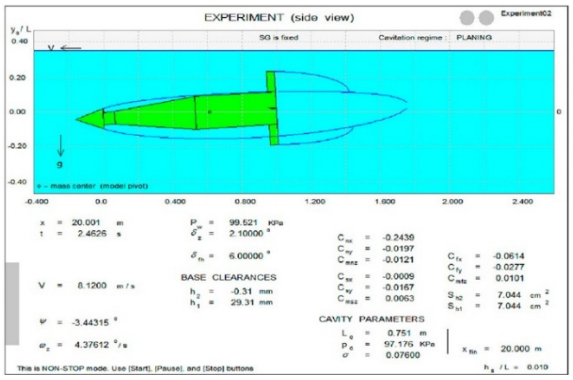

a

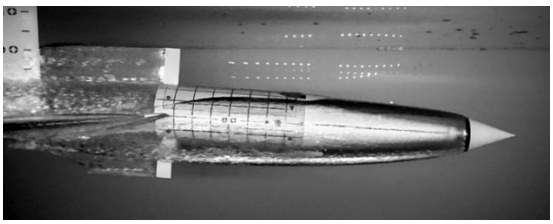

b

Fig. 15. Regime of planing of the model along the upper cavity wall: (*a*) – calculation; (*b*) – experiment

Conclusions

Experimental studies of the rotary cone cavitators were carried out at the high-speed experimental tank of the IHM of the NAS of Ukraine. Based on the obtained test results, the approximate dependences of both the drag coefficient c_x and the lift coefficient c_y of an inclined cone cavitator on the rotary angle δ for the wide range of the cone angles β_n have been proposed.

It was shown that the cone cavitators are more efficient operating controls than the equivalent disk cavitator for the cone angles $\beta_n < 65.4°$. With the help of computer simulation, a number of problems of dynamics of the SC-vehicles with the cone cavitators were studied: balancing the SC-vehicle, the motion stabilization, maneuvering the SC-vehicle, the cavity control.

The method of control of the SC-vehicle cavity by regulating the cavitator cone angle was proposed and investigated. It was shown that it is possible to compensate (within certain limits) the cavity dimension variation caused by varying the velocity $V(t)$ and/or immersion depth $H(t)$ of the SC-vehicle motion by regulating the angle $\beta_n(t)$. It can be shown that this method is more efficient than the known method of the ventilated cavity control by regulating the gas-supply.

For the first time, an experimental verification of the mathematical model of the SC-vehicle dynamics "as a whole" was performed by testing the model with the disk cavitator and the cone cavitators and the cavity-piercing fins with a degree of freedom in pitch. Comparison of the kinematic characteristics of the SC-vehicle model, obtained experimentally and by calculation, shows that the developed mathematical model describes the SC-vehicle dynamic characteristics adequately and with sufficient accuracy for practice.

References

[1] G.V. Logvinovich, *Hydrodynamics of free-boundary flows*, Kyiv, Ukraine: Naukova Dumka, 1969, 208 p.

[2] G.V. Logvinovich and V.V. Serebryakov, "On methods for calculating a shape of slender axisymmetric cavities", *J. of Hydromechanics*, no. 32, pp. 47–54*,* 1975.

[3] V.N. Semenenko, "Artificial cavitation. Physics and calculations", *RTO-AVT/VKI Special Course on Supercavitating Flows*. February 12–16, 2001, VKI, Brussels (Belgium).

[4] V.N. Semenenko and Ye.I.Naumova, "Study of the supercavitating body dynamics", in *Supercavitation: Advances and Perspectives*, Springer-Verlag, Berlin and Heidelberg, 2012, pp. 147–176. doi: 10.1007/978-3-642-23656-3_9

[5] V.N. Semenenko, "Analysis of the supercavitating body dynamics and control basing on the G.V.Logvinovich theory", *J. of Applied Hydromechanics*, vol. 15, no. 1, pp. 83–93, 2013.

[6] E.V. Paryshev, "Numerical modeling of pulsation of ventilated cavities", *Trudy TSAGI*, No. 2272, pp.19–28, 1985.

[7] V.N. Buyvol, *Slender cavities in perturbed flows*, Kyiv, Ukraine: Naukova Dumka, 1980, 296 p.

[8] L.G. Gusevsky, "Approximation dependences for axi-symmetric cavities behind cones", in *Hydroynamic flows and wave processes*, ITF SO AN SSSR, Novosibirsk, 1983, pp. 82–91.

[9] E.V. Paryshev, "On unsteady planing of a body over liquid curvilinear surface", *Second Int. Summer Scientific School "High Speed Hydrodynamics"*, Cheboksary, Russia, pp. 175–178, 2004.

[10] Yu.N. Savchenko and V.N. Semenenko, "Motion of supercavitating vehicle during underwater speeding-up", *J. of Applied Hydromechanics*, vol. 17(89), no. 4, pp. 36–42, 2015.

[11] V.N. Semenenko and O.I. Naumova, "Dynamics of a partially cavitating underwater vehicle", *J. of Hydrodynamics and Acoustics*, vol. 1 (91), no. 1, pp. 70–84, 2018. doi: 10.15407/jha2018.01.070

[12] V.N. Semenenko and O.I. Naumova, “Some ways of hydrodynamic fin application for underwater supercavitating vehicles”, *J. of Hydrodynamics and Acoustics*, vol. 1 (91), no. 3, pp. 355–371, 2018. doi: 10.15407/jha2018.03.355

[13] Yu.N. Savchenko, V.N. Semenenko, and G.Yu. Savchenko, “Peculiarities of maneuvering at the supercavitating flow”, *J.* of Applied Hydromechanics, vol. 18, no. 1, pp. 79–82, 2016.

[14] Yu.N. Savchenko, V.N.Semenenko, and G.Yu. Savchenko, “Peculiarities of supercavitating vehicles’ maneuvering”, *International J. of Fluid Mechanics Research*, vol. 46, no. 4, pp. 309–323*,* 2019. doi: 10.1615/InterJFluidMechRes.v46.i4.30

[15] T. Kiceniuk, “An experimental study of the hydrodynamic forces acting on family of cavity-producing conical bodies of revolution inclined to the flow”, *Report No. E–12–17*, Hydrodynamics Laboratory, California Institute of Technology. Pasadena, California, 1954.

[16] V. Kochin, V. Moroz, V. Serebryakov, and N. Nechitailo. “Hydrodynamics of Supercavitating Bodies at an Angle of Attacks under Conditions of Considerable Effect of Fluid Weightiness and Closeness of Free Border”, *J. of Shipping and Ocean Engineering*, no.5, pp. 255 –265, 2015. doi:10.17265/2159-5879/2015.05.004

[17] V.V. Serebryakov, V.V. Moroz, V.A. Kochin, and J. E. Dzielski, “Experimental Study on Planing Motion of a Cylinder at Angle of Attack in the Cavity Formed behind an Axisymmetric Cavitator”, *J. of Ship Research*, vol. 64, no.2, pp.139 –153, 2020. doi: 10.5957/JOSR.09180077

[18] V. Kochin, V. Moroz, V. Semenenko and Paik Bu-Geun, “Experimental verification of mathematical model of the supercavitating underwater vehicle dynamics”, *The 11th International Symposium on Cavitation CAV2021*, DCC, Daejeon, Korea, May 9–13, 2021.

[19] Testing and Extrapolation Methods. High Speed Marine Vehicles. Resistance Tes,” *ITTC – Recommended Procedures and Guidelines* No. 7.5-02 -05-01, 25th ITTC 2008.

[20] V. Kochin and V. Moroz, “Automated data acquisition and processing system for a high-speed towing tank”, *Modern* technologies of automation, no. 3, pp. 48-50, 2009.

[21] A. May, “Water entry and the cavity-running behavior of missiles”, *SEAHAC Technical Report 75-2, Naval Surface Weapons Center, White Oak Laboratory*, Silver Spring, MD, 1975. doi: 10.21236/ADA020429

[22] L.A. Epshtein. Methods of theory of dimensionalities and similarity in problems of ship hydromechanics. Leningrad: Sudostroenie Publ., 1970, 208 p.

[23] Yu.N. Savchenko and G.Yu. Savchenko, “Estimate of efficiency of supercavitation using on the axisymmetric hulls”, *J. of Applied Hydromechanics*, vol. 6, no. 4, pp. 78–83, 2004.

[24] H. Schlichting. *Boundary layer theory*. New York, 1961, 740 p.

[25] Yu.N. Savchenko and V.N. Semenenko, “Special features of supercavitating flow around polygonal contours”, *International J. of Fluid Mechanics Research*, vol. 28, no. 5, pp. 660– 672*,* 2001. doi: 10.1615/InterJFluidMechRes.v28.i5.60

[26] J. Dzielski and A. Kurdila, “A benchmark control problem for supercavitating vehicles and an initial investigation of solution”, *J. of Vibration and Control*, no. 19(7), pp. 791– 804, 2003. doi: 10.1177/1077546303009007004

[27] V.M. Semenenko and O.I. Naumova, “Motion of underwater supercavitating vehicles along the assigned paths”, *The XI* All-Ukrainian Scientific and Technical Conference “Underwater Technique and Technology”, Mykolaiv, Ukraine, December 02–03, 2021.

[28] Yu.N. Savchenko, Yu.D. Vlasenko, and V.N. Semenenko. “Experimental study of high-speed cavitated flows, *International J. of Fluid Mechanics Research*, vol.26, no. 3, pp. 365-374, 1999. doi: 10.1615/InterJFluidMechRes.v26. i3.80

Динаміка суперкавітуючих апаратів з конусними кавітаторами

В.Семененко, В. Мороз, В. Кочин, О. Наумова

Анотація. *Робота присвячена теоретичному та експериментальному дослідженню динаміки високошвидкісних підводних суперкавітуючих апаратів з конусними кавітаторами, які розглядаються як орган управління рухом апарату. Використано математичну модель "тонкої" нестаціонарної каверни, засновану на принципі незалежності розширення перерізів каверни Г.В. Логвіновича. Проведено експериментальні дослідження поворотних конусних кавітаторів у швидкісному дослідному басейні Інституту гідромеханіки НАН України. За результатами випробувань запропоновано апроксимаційні залежності коефіцієнтів опору та поперечної сили поворотних конусних кавітарів від кута повороту в широкому діапазоні кутів конусності. Визначено діапазон кутів конусності, для якого конусні кавітатори є ефективнішими органами управління порівняно з еквівалентним дисковим кавітатором. За допомогою комп'ютерного моделювання досліджено ряд задач динаміки суперкавітуючих апаратів з конусними кавітаторами: балансування апарату, стабілізація руху, маневреність апарату, управління каверною. Вперше виконано експериментальну верифікацію математичної моделі динаміки суперкавітуючого апарату “в цілому” при випробуванні моделей з дисковим та конусними кавітаторами та рулями, що мають ступінь свободи по тангажу.*

Ключові слова: *суперкавітуючий апарат, конусний кавітатор, математична модель, комп'ютерне моделювання, експериментальні дослідження.*